Topological band evolution between Lieb and kagome lattices

Wei Jiang, Meng Kang, Huaqing Huang, Hongxing Xu, Tony Low, and Feng Liu

Phys. Rev. B **99**, 125131 — Published 18 March 2019

DOI: 10.1103/PhysRevB.99.125131

Topological band evolution between Lieb and Kagome lattices

Wei Jiang,[1,2] Meng Kang,[3] Huaqing Huang,[1] Hongxing Xu,[3,4] Tony Low,[2] and Feng Liu[1,*]

[1] *Department of Materials Science & Engineering, University of Utah, Salt Lake City, UT 84112, USA*
[2] *Department of Electrical & Computer Engineering, University of Minnesota, Minneapolis, Minnesota 55455, USA.*
[3] *School of Physics and Technology, Center for Nanoscience and Nanotechnology, and Key Laboratory of Artificial Micro- and Nano-structures of Ministry of Education, Wuhan University, Wuhan 430072, China*
[4] *The Institute for Advanced Studies, Wuhan University, Wuhan 430072, China*

(Dated: February 12, 2019)

Among two-dimensional lattices, both Kagome and Lieb lattices have been extensively studied, showing unique physics related to their exotic flat and Dirac bands. Interestingly, we realize that the two lattices are in fact interconvertible by applying strains along the diagonal direction, as they share the same structural configuration in the unit cell, *i.e.*, one corner-site and two edge-center states. We study phase transitions between the two lattices using the tight-binding approach and propose one experimental realization of the transitions using photonic devices. The evolution of the band structure demonstrates a continuous evolution of the flat band from the middle of the Lieb band to the top/bottom of the Kagome band. Though the flat band is destroyed during the transition, the topological features are conserved due to the retained inversion symmetry, as confirmed by Berry curvature, Wannier charge center, and edge state calculations. Meanwhile, the triply degenerate Dirac point (M) in the Lieb lattice transforms into two doubly degenerate Dirac points with one of which moves along M-Γ and the other moves along M-K/K' directions that form the Kagome band eventually. Interestingly, the Dirac cones in the transition states are strongly tilted, showing a coexistence of type-I and type-II Dirac points. We finally show that these transitions can be experimentally realized in photonic lattices using waveguide arrays.

I. INTRODUCTION

The band theory has empowered us to understand most fundamental electronic properties of solid state systems[1,2]. For most generic cases, the energy, $E_n(k)$, is a parabolic function of k [$E_n(k) \propto k^2$], from which the effective mass and velocity of the quasi-particle can be derived. These have been widely applied to semiconductors, *e.g.*, Si and Ge, to calculate their electrical conductivity[3–5]. There are also exotic bands where $E_n(k)$ is a linear function of k [$E_n(k) \propto k^1$] or a constant independent of k [$E_n(k) \propto k^0$]. The famous example for the former scenario is discovered in the two-dimensional (2D) crystal, graphene, where the π states form linear dispersive bands (Dirac state) around the Fermi level[6–8]. Such a linear relationship between $E_n(k)$ and k gives rise to massless relativistic particles, leading to peculiar electronic properties, such as semimetallic state with extremely high electron mobility, and recently intensively studied topological properties[9–12].

The latter scenario with a constant $E_n(k)$, so called flat band, have been studied for decades[13,14]. It is known for its completely quenched kinetic energy and can be generally categorized into two classes, *i.e.*, localized state and itinerant state with destructive interference. The localized states are common but typically trivial, which can be viewed as isolated states without interaction, such as dangling bond or the defect state in semiconductors[15–17]. The flat bands formed by destructive interference are quite rare, which normally have stringent symmetry and coupling requirement, such as in the 2D Kagome[18], Lieb[19] and most recently discovered coloring-triangle (CT)[20] lattices. Because of nonvanishing interaction and strong correlation involved, such flat band systems have been proposed to realize high temperature ferromagnetism, superconductivity, and topological states[21–24]. Specifically, because of the vanishing bandwidth of the flat band with nontrivial topology and strong Coulomb repulsion, if the bandwidth is smaller than the band gap, then high temperature fractional quantum Hall state can appear upon partial filling of the flat band[25–27].

Though quite rare, there are a few 2D systems where both Dirac and flat band coexist, such as the Kagome, Lieb, Dice and CT lattices[18–20,28]. However, the arrangement of the Dirac bands and the flat band are quite different. In the Lieb lattice, the flat band is located in the middle of the Dirac bands, while in the Kagome lattice, the flat band is located either at the top or the bottom of the Dirac bands. Interestingly, we find that the Kagome and Lieb lattices are interconvertible by applying strains along the diagonal direction, as they share the same structural configuration in the unit cell, *i.e.*, one corner-site and two edge-center states [Fig. 1(a)]. It is interesting to understand the band transformation between the two lattices and also examine the topological properties in the transition state.

In this work, we first apply the tight-binding method to study the phase transition between the Lieb and the Kagome lattices. It is shown that the flat band is destroyed during the transition, due to symmetry breaking. Meanwhile, the triply degenerate M point splits into two different Dirac points; one moves toward Γ point and the other moves toward K/K' points. The topological properties of the system is conserved at both 1/3 and 2/3 fillings, as confirmed from our surface state, Wannier charge center, and Chern number calculations. The symmetry analysis show that the inversion symmetry play an important role in protecting the topological properties. Furthermore, we demonstrate the realization of such a phase transition in photonic lattices.

II. TIGHT-BINDING CALCULATIONS

We start from a single-orbital tight-binding model on the 2D edge-centered square lattice, *i.e.*, the Lieb lattice with the D_{4h} group symmetry. Each unit cell has one corner site B and two edge-center sites A and C, as shown in Fig. 1(a). The spinless Hamiltonian is defined as:

$$\mathcal{H}_0 = \sum_i \epsilon_i c_i^\dagger c_i + \sum_{\langle i,j\rangle} t c_i^\dagger c_j + \sum_{\langle\langle i,j\rangle\rangle} t_{ij} c_i^\dagger c_j + H.C., \tag{1}$$

where $c_i^\dagger$ and c_i are the creation and annihilation operators of an electron on the site i, t and t_{ij} represent the hopping amplitude between the nearest-neighbor (NN) $\langle i,j\rangle$ and the next-nearest-neighbor (NNN) $\langle\langle i,j\rangle\rangle$ sites, respectively. The NNN hopping term t_{ij} is defined as

$$t_{ij} = t \cdot e^{(\frac{a_0 - a_{ij}}{a_0})^n}, \tag{2}$$

with a_0 and a_{ij} representing the distance between NN and NNN sites. The exponent n controls how fast the hopping strength decays as a function of distance. Essentially, a larger n will yield a flatter band while a smaller n can better capture the evolution of the band structure from Lieb to Kagome. We have tested a few choices and found $n = 8$ to give both relatively flat bands and smooth transitions between the two lattices. It is known that the NNN interaction

affects the flatness of the flat band[29,30], whose effect has been supressed using Eq. (2) here. The hoppings beyond the NNN are neglected for simplicity. ϵ_i is the on-site energy on site i, which is set to 0. We note that the on-site energy difference between corner and edge-center site changes the degeneracy of the Dirac points[29,31], which however will not be discussed here. The band structure of Eq. (1) can be obtained by transforming $\mathcal{H}_0$ into momentum space as: $\mathcal{H} = \sum_k \Psi_k^\dagger H(k) \Psi_k$ with $\Psi_k^\dagger = (c_{Ak}^\dagger, c_{Bk}^\dagger, c_{Ck}^\dagger)$ and

$$H(k) = \begin{pmatrix} 0 & -2tcos(\overrightarrow{k} \cdot \frac{\overrightarrow{v_1}}{2}) & -2tcos(\overrightarrow{k} \cdot \frac{\overrightarrow{v_2}}{2}) \\ & 0 & -2t_{AC}\{cos[\overrightarrow{k} \cdot \frac{(\overrightarrow{v_1}-\overrightarrow{v_2})}{2}] + cos[\overrightarrow{k} \cdot \frac{(\overrightarrow{v_1}+\overrightarrow{v_2})}{2}]\} \\ & & 0 \end{pmatrix},$$

where $\overrightarrow{v_1}$ = (1, 0) and $\overrightarrow{v_2}$ =(0, 1) are the unit vectors that define the displacement vectors. $\overrightarrow{k} = (k_x, k_y)$ is the reciprocal lattice k vector. The lower triangle of the matrix should be filled accordingly for a Hermitian matrix, which is not shown.

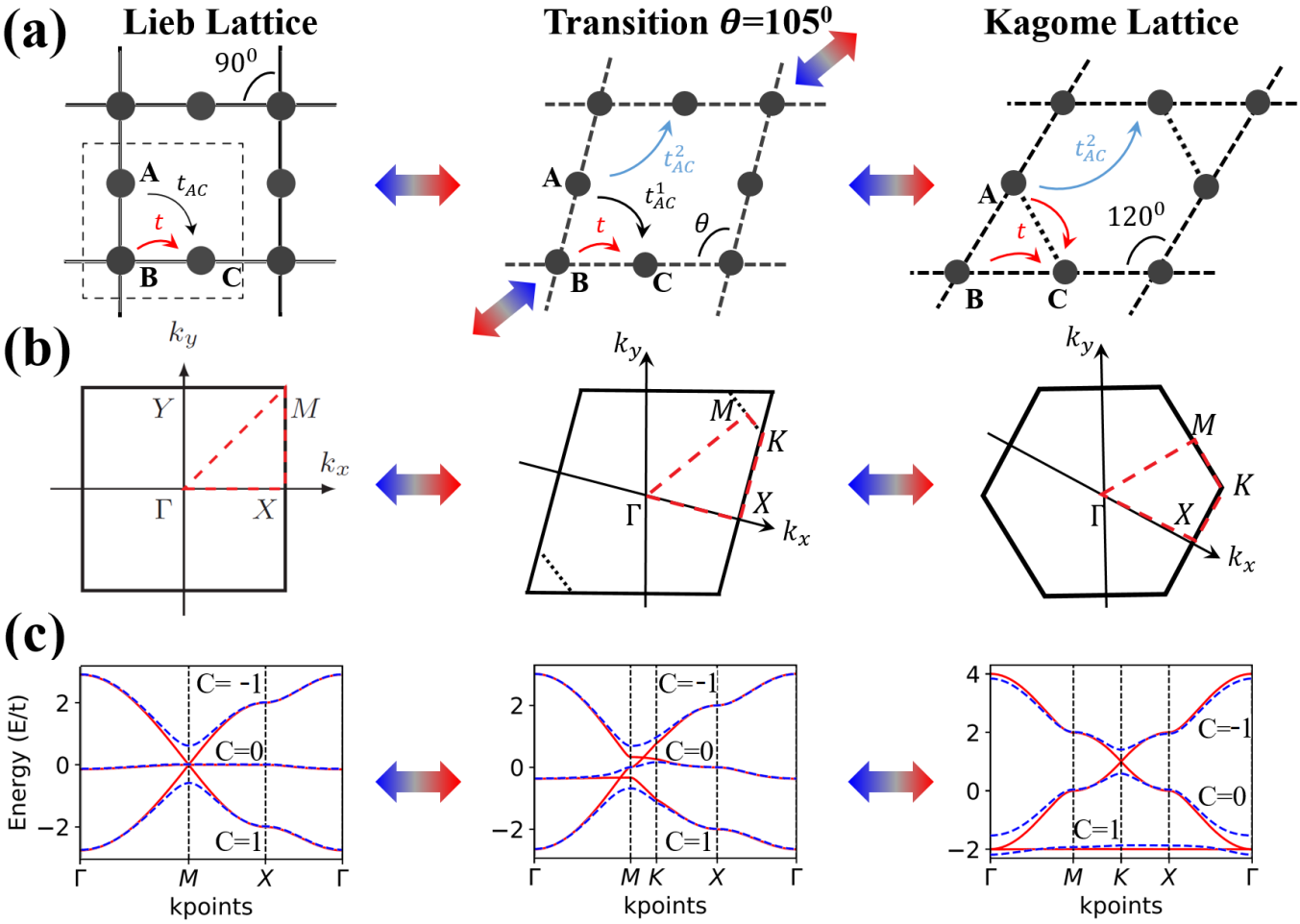

FIG. 1. Tight binding model for the transition between Lieb and Kagome lattices. (a) Structures of the Lieb lattice, transition lattice with θ=105°, and Kagome lattice. (b) The corresponding first-Brillouin zone for the three lattices with high-symmetry K-paths highlighted by red dashed lines. (c) The band structure along high-symmetry paths for the three lattices with (blue dashed lines) and without spin-orbit coupling (red solid lines). The Chern numbers for each band are labelled. Blue/red arrows indicate compressive/tensile strain along the diagonal direction.

When applying compressive/tensile strain along the diagonal direction [Fig. 1(a)], the square unit cell becomes orthorhombic with a group symmetry of D_{2h}. The lattice can be defined by two new unit vectors $\overrightarrow{v_1} = (1, 0)$ and $\overrightarrow{v_2} = (-cos\theta, sin\theta)$, with the angle θ in the range of $[\pi/2, 2\pi/3]$. Apparently, the lattice represents the Lieb and Kagome lattice when θ equals to $\pi/2$ and $2\pi/3$, respectively [Fig. 1(a)]. The two symmetric hopping between A and

C sites in the Lieb lattice become asymmetric when θ does not equal to $\pi/2$. Therefore, the NNN term is modified to a more general form: $-t^1_{AC}\,cos[\overrightarrow{k}\cdot(\overrightarrow{v_1}-\overrightarrow{v_2})/2]-t^2_{AC}\,cos[\overrightarrow{k}\cdot(\overrightarrow{v_1}-\overrightarrow{v_2})/2]$, where t^1_{AC} and t^2_{AC} are defined using Eq. (2). It is important to mention that when θ equals to $2\pi/3$, t^1_{AC} between A and C sites becomes equal to the NN hopping t. t^2_{AC} becomes the only NNN interaction, which has negligible effect according to Eq. (2). With the change of θ from $\pi/2$ to $2\pi/3$, the first-Brillouin zone changes gradually from square to hexagonal parallelogon to regular hexagon, as shown in Fig. 1(b). We note that even with different θ, the inversion symmetry of the lattice remains. This is crucial for their nontrivial topological properties, which will be discussed later.

Band evolution. We plot band structures for the three lattices along the high-symmetry k-paths, as shown in Fig. 1(c). The left and right panels of Fig. 1(c) show the well-known features of Lieb and Kagome bands, characterized by the coexistence of Dirac bands and flat band. The flat band locates at the middle of the Dirac bands in the Lieb band, while at the bottom in the Kagome band[25,32]. It is worth mentioning that with different signs of the hopping integral, the flat band in the Kagome band can sit either at the top or bottom of the Dirac band, which can be understood by considering the local magnetic flux[33,34]. Looking at the band structure of the transition state [middle panel of Fig. 1(c)], one sees the flat band disappeared. This is reasonable because the formation of flat band in the Lieb and Kagome lattice is due to the destructive interference or phase cancellation of Bloch wavefunctions caused by lattice symmetry. Such delicate condition is broken by lattice distortion that breaks the required symmetry for flat band.

On the other hand, we notice that the triply degenerate M point splits into two doubly degenerate Dirac points located along the Γ-M and M-K/K' paths, respectively. As θ changes from $\pi/2$ to $2\pi/3$, one of the Dirac points moves from the M to Γ point on the M-Γ path, and the other moves from the same M point to the K/K' point on the M-K/K' path (see Appendix Fig. 7 and supplementary video[35]). Compared with the Dirac cones in the Lieb and Kagome lattice, the Dirac cones in the transition state are strongly tilted. More interestingly, the transition state hosts two types of Dirac points with different features, *i.e.*, type-I, a point-like Fermi surface, and type-II, where the Dirac point locates at the contact of the electron and hole pockets[36,37]. There are proposals that the transition state between the type-I and type-II Dirac points represents a solid-state analog of the black-hole-horizon, which could possibly be used to simulate black-hole radiation[38,39]. As the band dispersion is tunable by varying the distortion (θ) and the NNN interaction, it is possible to realize the transition between type-I and type-II by straining either a Kagome or Lieb lattice. We will briefly illustrate this possibility in photonic devices at the end.

Topological properties. Next, we study the topological properties of the lattices in transition by adding an intrinsic spin-orbit coupling (SOC) interaction:

$$\mathcal{H}_{soc}=i\lambda_{ij}\sum_{\langle i,j\rangle}v_{ij}c_i^\dagger\sigma_z c_j+i\lambda_{ij}\sum_{\langle\langle i,j\rangle\rangle}v_{ij}c_i^\dagger\sigma_z c_j+H.C., \tag{3}$$

where both NN and NNN SOC are considered with the amplitude of λ_{ij} defined as $\lambda e^{(\frac{a_0-a_{ij}}{a_0})^n}$. λ is set to be $0.05t$. v_{ij} is defined as $d^1_{ij}\times d^2_{ij}$, where d^1_{ij} and d^2_{ij} are the two vectors along the NN bonds connecting sites i and j. n is again set as 8 for consistency. It is important to mention that for the Lieb lattice, the NN SOC respects the four-fold rotational symmetry and will not lift the degeneracy of the Dirac point to open a gap. In contrast, the NNN SOC would break the symmetry that leads to gap opening [Fig. 1(c)]. This is further confirmed when we break the D_{4h} symmetry by applying strain along diagonal direction. The lattice now possesses D_{2h} symmetry, which opens a finite gap at both Dirac points even when only the NN SOC coupling is included, as shown in the middle panel of Fig. 1(c). The same behaviors are also observed in the Kagome lattice with the D_{6h} symmetry.

The gap opening by the SOC effect indicates the lattice to be topologically nontrivial. To further reveal the topological properties of the lattice, we then calculate the edge state of a finite ribbon system (with a ribbon width of 15 units). Figure 2 shows clearly the edge states that connect the bulk states within both gaps. Since we are using a spinless Hamiltonian, only one spin-polarized edge state exists in the gap. When we consider both the spin-up and spin-down components, these topological edge states will form a 1D Dirac cone within the gap. The red and blue colors of the edge states in Fig. 2(a) represent the contributions from two sides of the ribbon respectively. This is further confirmed by our edge-state eigenfunction plot, as shown in Fig. 2(b). It is known that the topological properties can also be characterized by the evolution of the charge centers of the hybrid Wannier function (Wannier charge centers, WCCs), which carries the same topological information as the surface energy bands[40,41]. Thus, we also plotted the WCCs of these three lattices at the 1/3 and 2/3 filling, as shown in Fig. 3. The shape of the WCCs changes smoothly from the Lieb lattice to the Kagome lattice through the transition state. They are consistent with the edge-state results, confirming the nontrivial topology.

Topological invariant The nontrivial topology of the systems can be further confirmed through the topological invariant calculation, *i.e.*, Chern number (C), using the Kubo formula[42,43]:

$$C=\frac{1}{2\pi}\int_{BZ}d^2\overrightarrow{k}\;\Omega(\overrightarrow{k}),\;\Omega(\overrightarrow{k})=\sum_n f_n\Omega_n(\overrightarrow{k}), \tag{4}$$

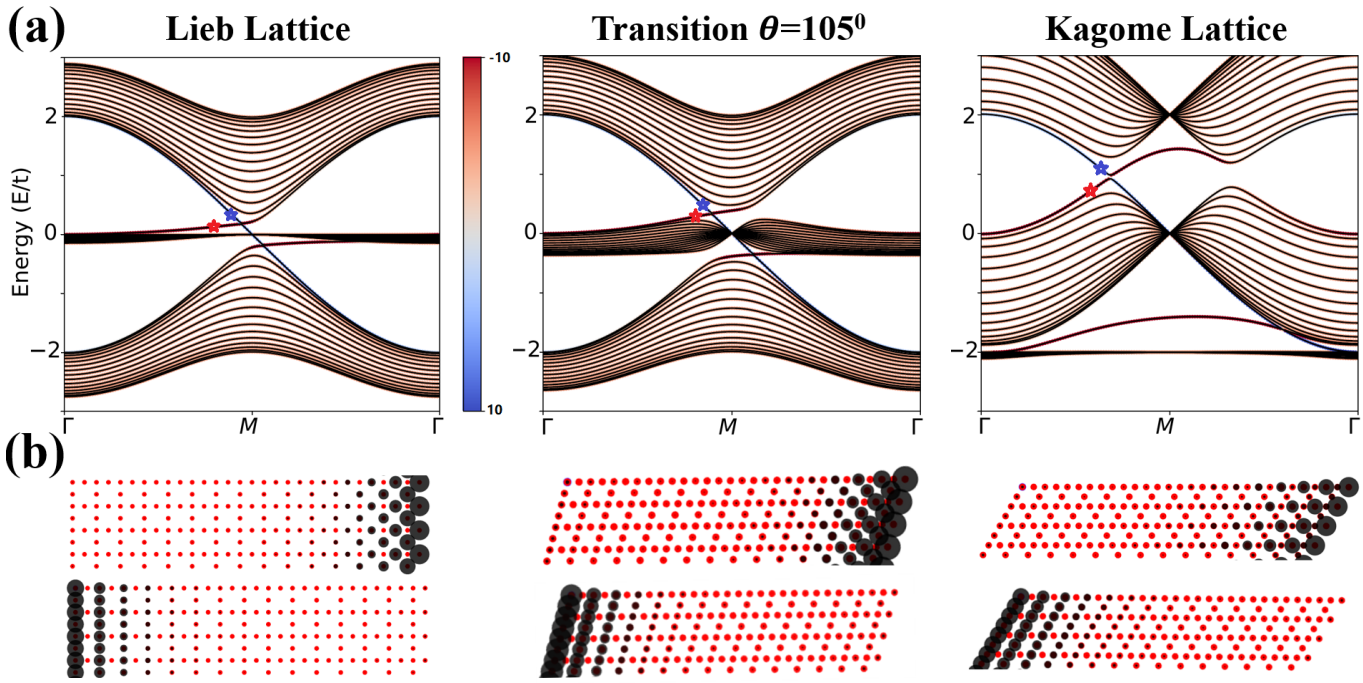

FIG. 2. Ribbon calculation. (a) Surface state of a finite ribbon system with a ribbon width of 15 units for Lieb, transition, and the Kagome lattices. (b) The upper and lower panel shows the wavefunction of the two edge-states within the bulk gap for the three lattices, with their corresponding k-points highlighted by the red and blue stars in (a), respectively. The size of the black dots represents the norm of the wavefunction.

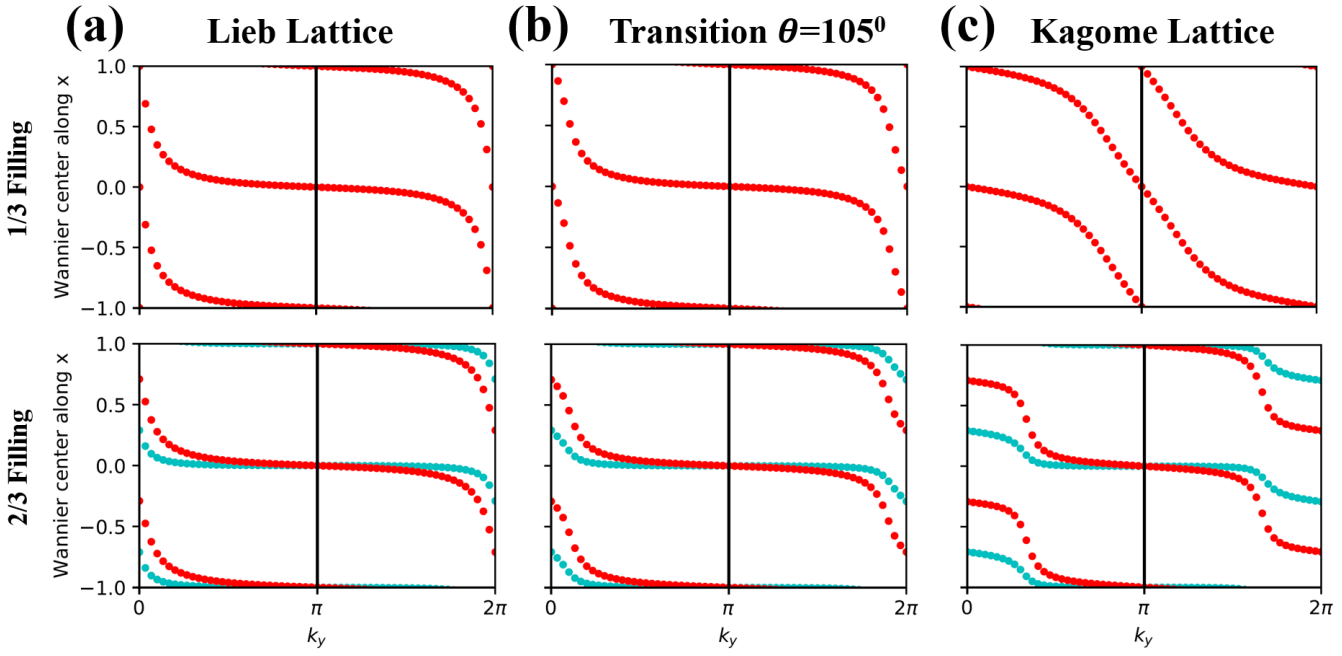

FIG. 3. Wannier charge centers. (a) Evolution of WCCs along the k_y direction integrated along x direction for the Lieb lattice. Upper and lower panels show the WCCs for 1/3 and 2/3 filling, respectively. (b) and (c) Same as (a) for the transition lattice and the Kagome lattice, respectively. The red and blue dots represent the first and second band, respectively.

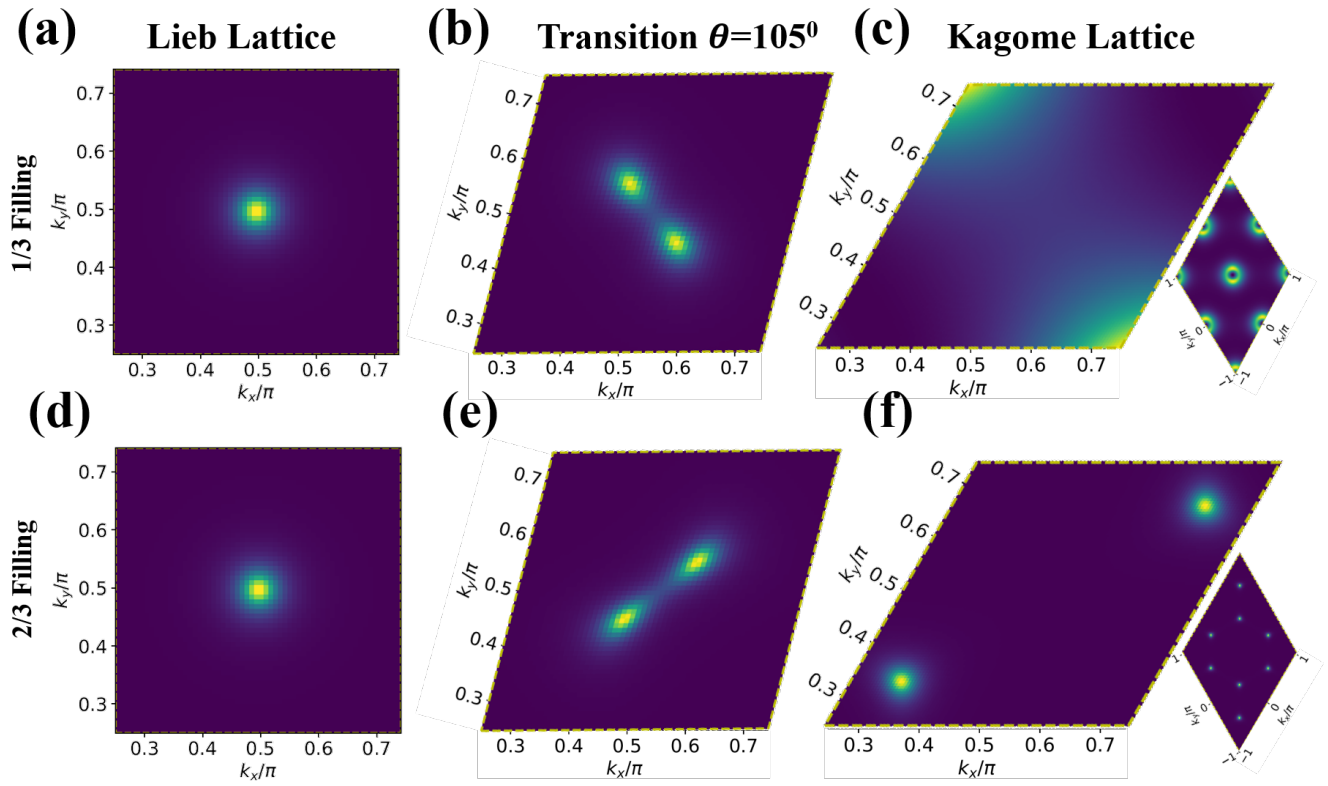

FIG. 4. Evolution of Berry curvature. (a)-(c) Berry curvature of the lower band for the Lieb lattice, transition state, and the Kagome lattice with 1/3 filling, respectively. The 2×2 unit cell Berry curvature plot shows the triangle lattice formed by Berry curvature peaks around the Γ point. (d)-(f) Same as (a)-(c) for the middle band with 2/3 filling. The 2×2 unit cell Berry curvature plot shows the hexagonal lattice formed by Berry curvature peaks around the K and K' points.

$$\Omega_n(\overrightarrow{k}) = -\sum_{n'\neq n} 2Im\frac{\langle\Psi_{nk}|\hat{\nu}_x|\Psi_{n'k}\rangle\langle\Psi_{n'k}|\hat{\nu}_y|\Psi_{nk}\rangle}{(\epsilon_{n'k}-\epsilon_{nk})^2}, \tag{5}$$

where n is the band index, Ψ_{nk} and ϵ_{nk} are the eigenstate and eigenvalue of the band n, respectively. f_n is the Fermi distribution function, $\hat{\nu}_{x/y}$ is the velocity operator. The Chern numbers of different bands for the three systems are labeled in Fig. 1(c), where the bottom and the top bands have a nonzero Chern number (±1) and the middle band has a zero Chern number. The Chern numbers are consistent with the number of quantized edge-states as observed in Fig. 2. Therefore, the two SOC gaps between the three bands are both topological nontrivial. This can also be confirmed by the Berry curvature plot, as shown in Fig. 4. It can be clearly seen that the nonzero Berry curvatures are mainly localized around the Dirac points, which become gapped due the SOC effect. As a consequence, the evolution of the Dirac points can also be directly visualized from the change of Berry curvatures for the three lattices. Fig. 4(a)-(c) depict the Berry curvatures for the bottom bands with 1/3 filling, where the peak (bright dot) splits from the M point into two points and move to the Γ point through the M-Γ path. While the Berry curvatures for the middle band with 2/3 filling [Fig. 4(d)-(f)] evolve from the M point to the K/K' point through the M-K/K'-path that is perpendicular to the M-Γ. In a 2×2 unit cell, Berry curvature plots for the Kagome lattice show clearly the triangle and hexagonal lattice formed by Berry curvature peaks at the Γ and K/K' points, respectively. These results are consistent with our Dirac points evolution in band structure calculations, when the Lieb lattice changes to the Kagome lattice, as shown in Fig. 1(c).

By analyzing the structural symmetry, we find that the lattice symmetry changes from D_{4h} to D_{2h} to D_{6h} when θ changes from $\pi/2$ to $2\pi/3$, all of which possess the inversion symmetry and the mirror symmetry with respect to both diagonal lines. To understand the topological origin, we first break the inversion symmetry by introducing a dimer interaction between the corner site (B) and edge-center sites (A, C), while keeping one mirror symmetry intact [Fig. 5(a)]. Such a dimer interaction can be easily introduced by shifting A, C away from the center-sites of the same amount, which act as staggered hopping terms $t_{i,j} = t + \Delta t, t_{j,i+1} = t - \Delta t$ in the Hamiltonian. As can be seen

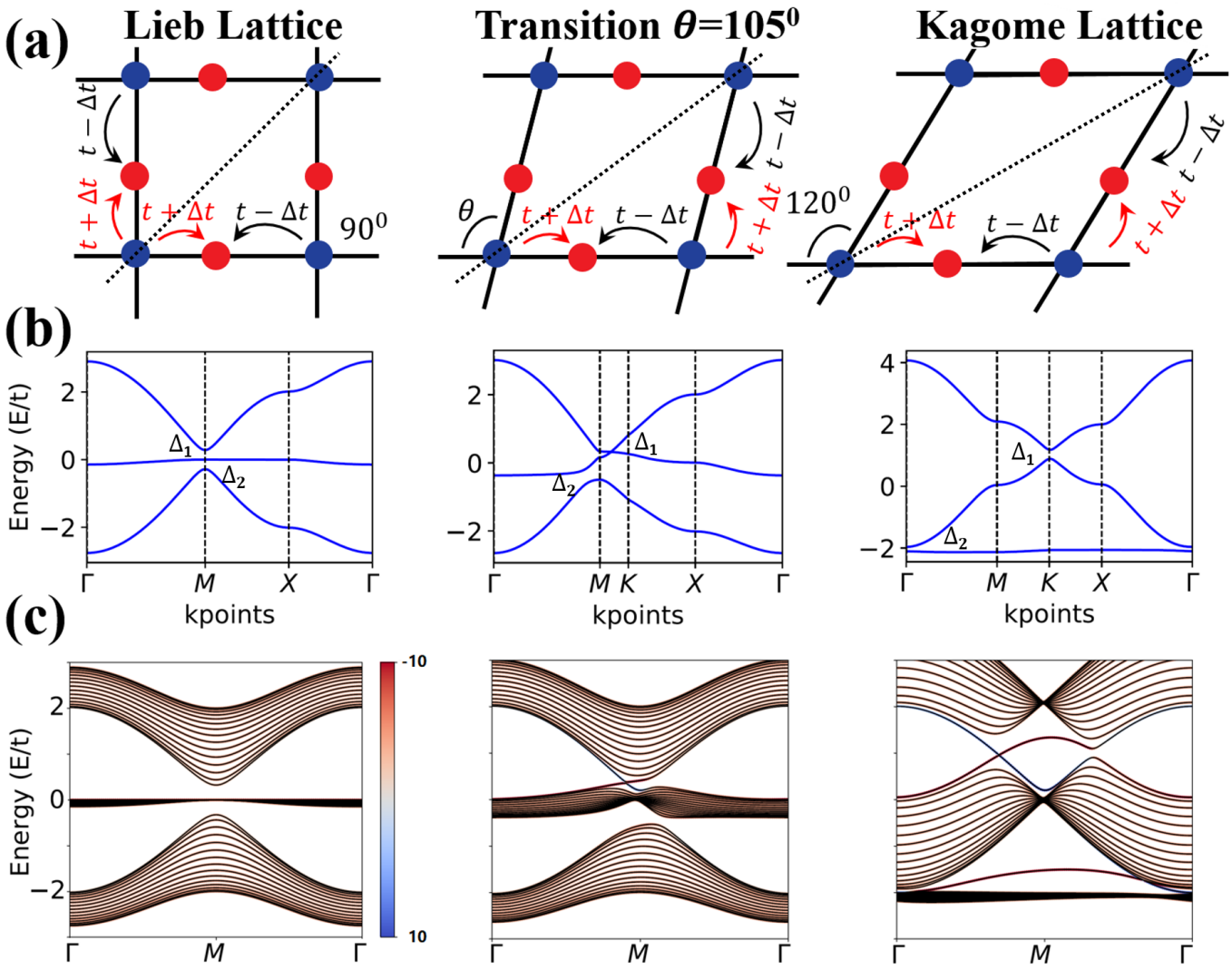

FIG. 5. Inversion symmetry broken lattices. (a) Structural configurations for the inversion symmetry broken lattices with one of the mirror symmetry intact, as highlighted by the dashed line. (b) Band structure of the corresponding lattices without SOC. (c) Ribbon band structures for the three lattices show the transition from the topological trivial state to the nontrivial state with the changes of θ.

from the band structures in Fig. 5(b), without considering SOC, the triply degenerate M point in the Lieb lattice splits in energy forming two gaps (Δ_1, Δ_2). Although it looks similar as the SOC effect [Fig. 1(c)], it is actually a topological trivial state with no signature of edge state in the ribbon band structure [left panel of Fig. 5(c)]. When one gradually increases θ, the band gap Δ_2 increases. Interestingly, however Δ_1 decreases and disappears at a certain θ value and reopens, indicating a band inversion and hence a topological transition. The gap opening mechanism of the Δ_1 for the Kagome lattice ($\theta = 2\pi/3$) is similar to that of the Δ_1 and Δ_2 for the Lieb lattice ($\theta = \pi/2$), which is due to breaking of the crystal symmetry, *i.e.*, D_{6h} and D_{4h} symmetry for Kagome and Lieb lattices, respectively. The interesting behavior of Δ_1 gap closing during the transition is due to the conservation of the mirror symmetry and the value of θ when the Δ_1 closes is determined by the strength of the dimer interaction, *i.e.*, the staggered hopping term Δt. The topological properties are further confirmed by the edge state calculations as shown in Fig. 5(c). For the transition state with θ equaling to 105°, only Δ_1 is topologically nontrivial; while for the Kagome lattice, both gaps are topologically nontrivial. When we further break the mirror symmetry by shifting A and C with a different amount away from the center-site, the system becomes fully gapped, leading to a completely topological trivial state.

III. PHOTONIC WAVEGUIDE SYSTEM

Next, we demonstrate the realization of band transition between Lieb and Kagome lattice in weakly coupled waveguide arrays. The periodic waveguides play the role of states with different potential, where photons in a photonic lattice behave similar as electrons in a crystal. In tight-binding approximation, time evolution for the diffraction of light in a 2D photonic lattice is described as:

$$i\partial_z \Psi_{mn}(z) = \sum_{m'n'} t_{m'n'} \Psi_{m'n'}(z), \tag{6}$$

where Ψ_{mn} is the field amplitude of the m, nth waveguide, $t_{m'n'}$ is the hopping term representing coupling strength between two neighboring waveguides, and z is the propagation direction. The corresponding three-band Hamiltonian is obtained as:

$$H^T(K) = \begin{pmatrix} 0 & t(1+e^{-ik\cdot v_2}) & t(1+e^{-ik\cdot v_1}) \\ & 0 & t'(1+e^{-ik\cdot(v_1-v_2)}) \\ & & 0 \end{pmatrix} \tag{7}$$

where t' is NNN hopping which is much smaller than t. The eigenvalue β, which represents the propagation constant in the z direction, can be solved by diagonalization.

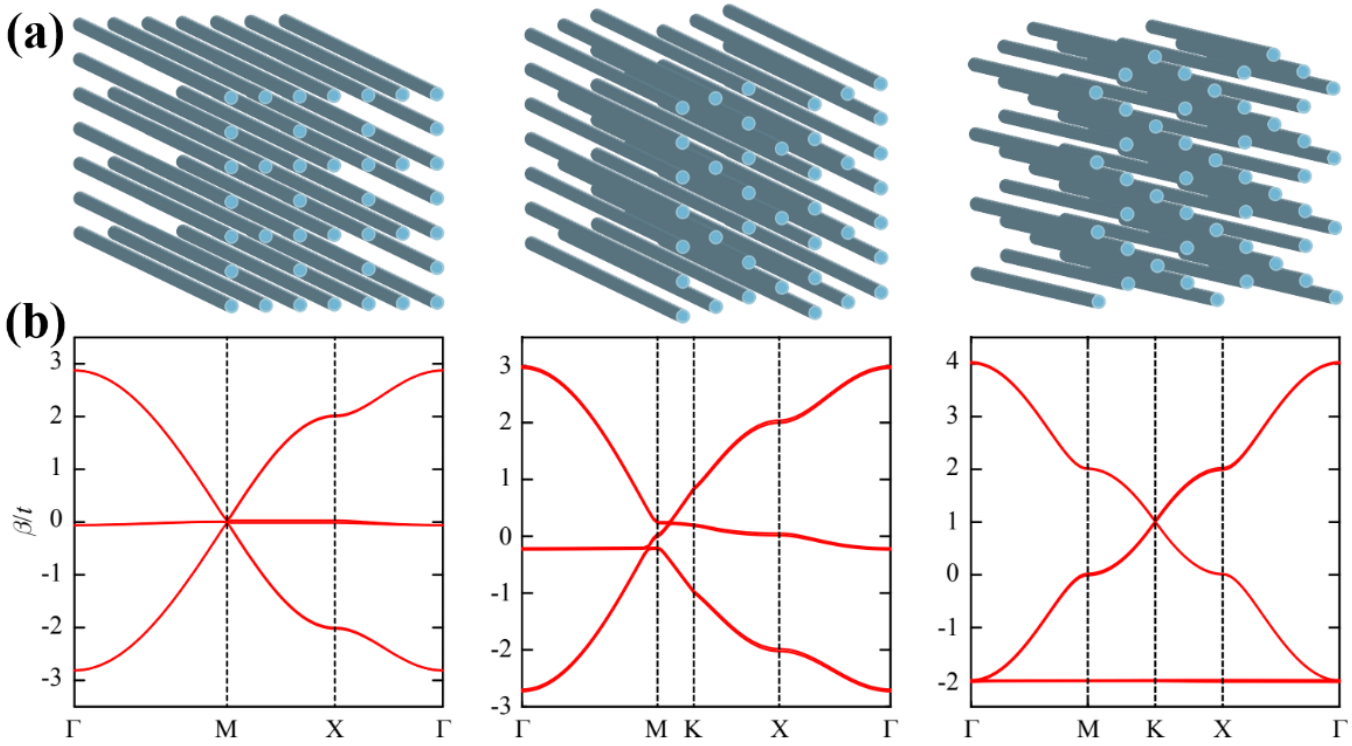

FIG. 6. Schematic diagram of waveguide systems. (a) Structures of the Lieb lattice, transition lattice with θ= 105° and Kagome lattice. The corresponding numerical simulated band structures are shown in (b).

We then carried out calculations to reveal the evolution of band structures from Lieb lattice to Kagome lattice by full-wave numerical simulations. As seen from Fig. 6(a), waveguides are arranged in a Lieb lattice, transition lattice with θ equals 105°, and Kagome lattice, respectively. Each waveguide only supports one single fundamental mode. The distance between two adjacent waveguides is tuned to make NNN hopping relatively small in the Lieb lattice. The diameter D of every waveguide is 4 μm and the distance d between two adjacent waveguides is 17 μm. The waveguide array has the perturbed refractive index δn = 0.003, and the wavelength of the laser is set to be 633 nm. Silica with a refractive index n_0 = 1.45 is used as the supporting media. These parameters in the simulations can be readily implemented experimentally via femtosecond direct-writing or optothermal nonlinearities method[44,45]. The band structures were constructed by mode analysis based on finite element method. The band structures of Lieb lattice,

transition lattice, and Kagome lattice are shown in Fig. 6(b), respectively, which agree with the electronic structure calculations. Topological properties of the system can be explored using periodically driven waveguides[46–48]. We note that hopping terms can also be tuned by a chain of waveguide[20,49], which could possibly be used to tune the band dispersion to realize the transition between type-I and type-II Dirac states. On the other hand, the Lieb and Kagome lattices have been separately proposed in real material systems, such as the 2D metal-organic and covelent-organic frameworks (MOF/COF)[24,50–53]. Considering the high tunability of the MOF/COFs[54,55], it is also possible to find suitable real 2D material systems to realize such phase transition. Analogue to the SOC in the electronic system, we can use gyro-magnetic materials as waveguide to break the symmetry of left-hand and right-hand polarized light; or use helical, instead of straight waveguides to break the z-reversal symmetry of the photonic lattice to achieve topological properties [56].

IV. CONCLUSION

In summary, we have implemented a tight-binding method to study the band transition between the Lieb and Kagome lattice, which is found to share the same structural configuration. Although the exotic flat band is destroyed in the transition states due to breaking of the D_{4h} and D_{6h} symmetry, the topological feature of the Dirac state is well preserved by the retained inversion symmetry. Further breaking inversion symmetry does not fully destroy the topological order, but instead lead to a surprising change of the topological origin because of the remaining mirror symmetry. The proposed photonic lattice and MOF/COFs systerms may serve as promising platforms to experimentally observe such an interesting topological band evolution.

Acknowledgement. This project is supported by U.S. DOE-BES (grant No. DE-FG02-04ER46148). WJ and TL acknowledge support in part by SMART, one of seven centers of nCORE, a Semiconductor Research Corporation program, sponsored by National Institute of Standards and Technology (NIST). W. J. is additionally supported by the NSF-Material Research Science & Engineering Center (grand No. DMR-1121252). M. K. and H. X. thank the financial support from the National Key Basic Research Program (Grant No. 2015CB932400) and the National Natural Science Foundation of China (Grant No. 11674256). M. K. acknowledges Wuhan University which supports him to visit University of Utah and participate this project. We thank the CHPC at the University of Utah and DOE-NERSC for providing the computing resources.

Appendix: Topological band evolution

* Corresponding author:fliu@eng.utah.edu

[1] C. Kittel, *Introduction to Solid State Physics*, 8th ed. (Wiley, 2004).
[2] O. K. Andersen, Phys. Rev. B **12**, 3060 (1975).
[3] D. L. Smith and C. Mailhiot, Rev. Mod. Phys. **62**, 173 (1990).
[4] I. Vurgaftman, J. R. Meyer, and L. R. Ram-Mohan, Journal of Applied Physics **89**, 5815 (2001).
[5] Z. Liu, J. Wu, W. Duan, M. G. Lagally, and F. Liu, Phys. Rev. Lett. **105**, 016802 (2010).
[6] K. S. Novoselov, A. K. Geim, S. V. Morozov, D. Jiang, M. I. Katsnelson, I. V. Grigorieva, S. V. Dubonos, and A. A. Firsov, Nature **438**, 197 (2005).
[7] A. H. Castro Neto, F. Guinea, N. M. R. Peres, K. S. Novoselov, and A. K. Geim, Rev. Mod. Phys. **81**, 109 (2009).
[8] G. E. I. M. A. K. and K. S. NOVOSELOV (Co-Published with Macmillan Publishers Ltd, UK, 2009) pp. 11–19.
[9] C. Lee, X. Wei, J. W. Kysar, and J. Hone, Science **321**, 385 (2008).
[10] Y. Zhang, Y.-W. Tan, H. L. Stormer, and P. Kim, Nature **438**, 201 (2005).
[11] C. L. Kane and E. J. Mele, Phys. Rev. Lett. **95**, 226801 (2005).
[12] C. L. Kane and E. J. Mele, Phys. Rev. Lett. **95**, 146802 (2005).
[13] T. D. Newton and E. P. Wigner, Rev. Mod. Phys. **21**, 400 (1949).
[14] P. W. Anderson, Phys. Rev. **109**, 1492 (1958).
[15] H. Kim, J. Lee, S.-J. Kahng, Y.-W. Son, S. B. Lee, C.-K. Lee, J. Ihm, and Y. Kuk, Phys. Rev. Lett. **90**, 216107 (2003).
[16] W. Jiang, Z. Liu, M. Zhou, X. Ni, and F. Liu, Phys. Rev. B **95**, 241405 (2017).
[17] L. Hu, H. Huang, Z. Wang, W. Jiang, X. Ni, Y. Zhou, V. Zielasek, M. G. Lagally, B. Huang, and F. Liu, Phys. Rev. Lett. **121**, 066401 (2018).
[18] A. Mielke, Journal of Physics A: Mathematical and General **24**, L73 (1991).
[19] E. H. Lieb, Phys. Rev. Lett. **62**, 1201 (1989).
[20] S. Zhang and et al., Unpublished (2018).

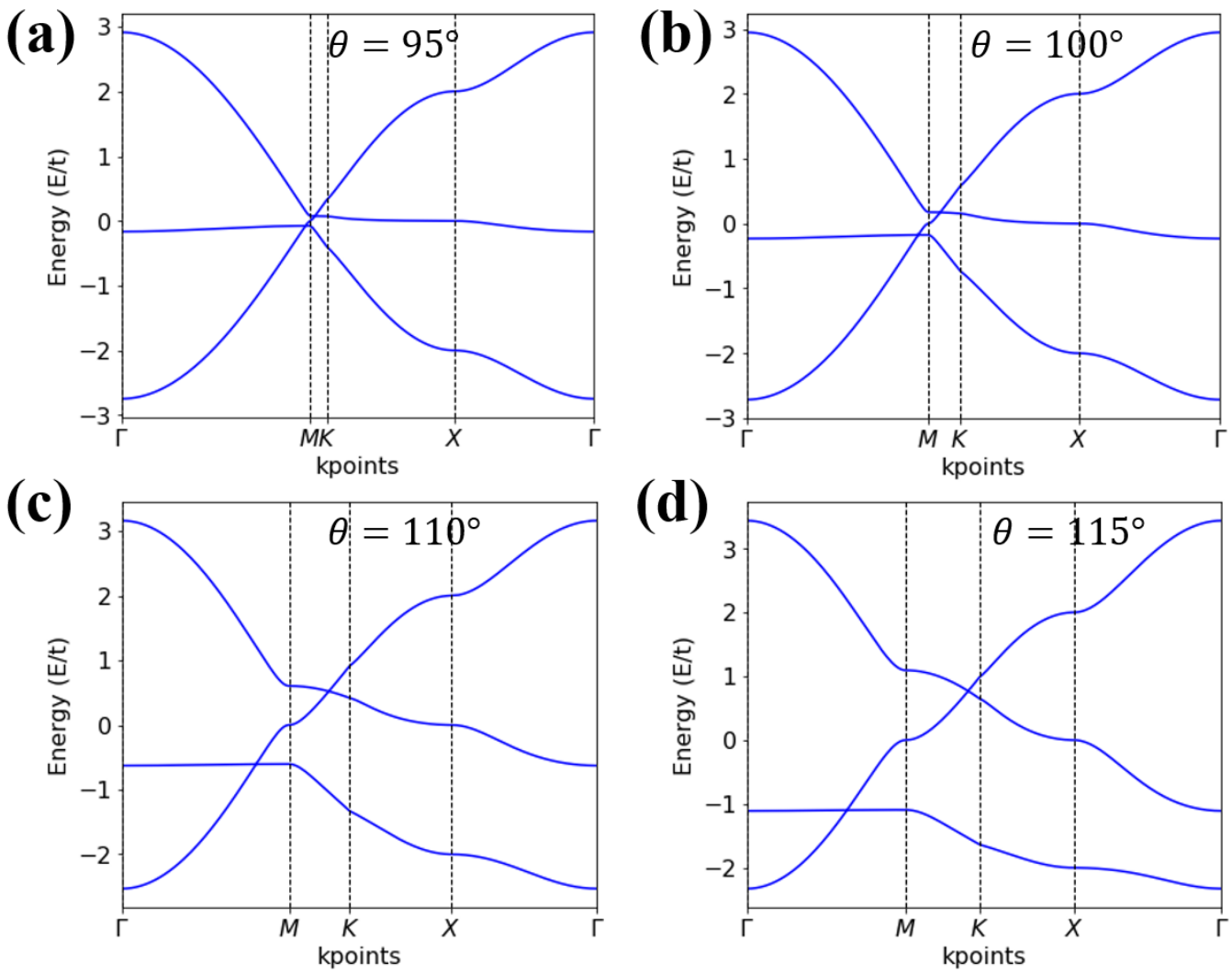

FIG. 7. Topological band evolution. Band structures for transition lattice with θ= (a) 95°, (b) 100°, (c) 110°, and (d) 115°.

[21] S. Depenbrock, I. P. McCulloch, and U. Schollwöck, Phys. Rev. Lett. **109**, 067201 (2012).
[22] T.-H. Han, J. S. Helton, S. Chu, D. G. Nocera, J. A. Rodriguez-Rivera, C. Broholm, and Y. S. Lee, Nature **492**, 406 (2012).
[23] Z. Liu, F. Liu, and Y.-S. Wu, Chinese Physics B **23**, 077308 (2014).
[24] W. Jiang, Z. Liu, J.-W. Mei, B. Cui, and F. Liu, Nanoscale (2018), 10.1039/C8NR08479C.
[25] E. Tang, J.-W. Mei, and X.-G. Wen, Phys. Rev. Lett. **106**, 236802 (2011).
[26] K. Sun, Z. Gu, H. Katsura, and S. Das Sarma, Phys. Rev. Lett. **106**, 236803 (2011).
[27] T. Neupert, L. Santos, C. Chamon, and C. Mudry, Phys. Rev. Lett. **106**, 236804 (2011).
[28] B. Sutherland, Phys. Rev. B **34**, 5208 (1986).
[29] W.-F. Tsai, C. Fang, H. Yao, and J. Hu, New Journal of Physics **17**, 055016 (2015).
[30] H. Ozawa, S. Taie, T. Ichinose, and Y. Takahashi, Phys. Rev. Lett. **118**, 175301 (2017).
[31] R. Chen and B. Zhou, Physics Letters A **381**, 944 (2017).
[32] C. Weeks and M. Franz, Phys. Rev. B **82**, 085310 (2010).
[33] K. Ohgushi, S. Murakami, and N. Nagaosa, Phys. Rev. B **62**, R6065 (2000).
[34] H.-M. Guo and M. Franz, Phys. Rev. B **80**, 113102 (2009).
[35] See Supplemental Material at [URL] for phase evolution vedio..
[36] Y. L. Chen, J.-H. Chu, J. G. Analytis, Z. K. Liu, K. Igarashi, H.-H. Kuo, X. L. Qi, S. K. Mo, R. G. Moore, D. H. Lu, M. Hashimoto, T. Sasagawa, S. C. Zhang, I. R. Fisher, Z. Hussain, and Z. X. Shen, Science **329**, 659 (2010).
[37] A. A. Soluyanov, D. Gresch, Z. Wang, Q. Wu, M. Troyer, X. Dai, and B. A. Bernevig, Nature **527**, 495 (2015).
[38] H. Huang, K.-H. Jin, and F. Liu, Phys. Rev. B **98**, 121110 (2018).
[39] H. Liu, J.-T. Sun, C. Cheng, F. Liu, and S. Meng, Phys. Rev. Lett. **120**, 237403 (2018).
[40] A. A. Soluyanov and D. Vanderbilt, Phys. Rev. B **83**, 235401 (2011).

[41] A. A. Soluyanov and D. Vanderbilt, Phys. Rev. B **83**, 035108 (2011).
[42] D. J. Thouless, M. Kohmoto, M. P. Nightingale, and M. den Nijs, Phys. Rev. Lett. **49**, 405 (1982).
[43] Y. Yao, L. Kleinman, A. H. MacDonald, J. Sinova, T. Jungwirth, D.-S. Wang, E. Wang, and Q. Niu, Phys. Rev. Lett. **92**, 037204 (2004).
[44] S. Shabahang, N. S. Nye, C. Markos, D. N. Christodoulides, and A. F. Abouraddy, Opt. Lett. **42**, 1919 (2017).
[45] A. Szameit and S. Nolte, Journal of Physics B: Atomic, Molecular and Optical Physics **43**, 163001 (2010).
[46] M. C. Rechtsman, J. M. Zeuner, Y. Plotnik, Y. Lumer, D. Podolsky, F. Dreisow, S. Nolte, M. Segev, and A. Szameit, Nature **496**, 196 (2013).
[47] S. Mukherjee, A. Spracklen, M. Valiente, E. Andersson, P. hberg, N. Goldman, and R. R. Thomson, Nature Communications **8**, 13918 (2017).
[48] L. Lu, J. D. Joannopoulos, and M. Soljai, Nature Photonics **8**, 821 (2014).
[49] G. G. Pyrialakos, N. S. Nye, N. V. Kantartzis, and D. N. Christodoulides, Phys. Rev. Lett. **119**, 113901 (2017).
[50] N. Su, W. Jiang, Z. Wang, and F. Liu, Appl. Phys. Lett. **112**, 033301 (2018).
[51] H. Chen, S. Zhang, W. Jiang, C. Zhang, H. Guo, Z. Liu, Z. Wang, F. Liu, and X. Niu, J. Mater. Chem. A **6**, 11252 (2018).
[52] X. Ni, W. Jiang, H. Huang, K.-H. Jin, and F. Liu, Nanoscale **10**, 11901 (2018).
[53] W. Jiang and et al., Unpublished (2018).
[54] H.-C. Zhou, J. R. Long, and O. M. Yaghi, Chem. Rev. **112**, 673 (2012).
[55] N. Stock and S. Biswas, Chem. Rev. **112**, 933 (2012).
[56] T. Ozawa, H. M. Price, A. Amo, N. Goldman, M. Hafezi, L. Lu, M. Rechtsman, D. Schuster, J. Simon, O. Zilberberg, and I. Carusotto, arXiv (2018), 1802.04173.